

Effect of Preaging Deformation on Aging Characteristics of 2507 Super Duplex Stainless Steel

M.K. Mishra, A.G. Rao, R. Sarkar, B.P. Kashyap, and N. Prabhu

(Submitted October 22, 2015; in revised form November 30, 2015; published online January 12, 2016)

In the present study, precipitation of sigma (σ) phase was investigated over the temperature range of 700–850 °C in undeformed and deformed (60% cold rolling) samples of 2507 super duplex stainless steel. The fraction of sigma phase formed as a result of the transformation $\alpha \rightarrow \sigma + \gamma_2$ increases with increasing time and temperature. The increase in sigma phase leads to increase in yield strength and decrease in ductility. Preaging deformation leads to accelerated precipitation of sigma phase. The activation energy for sigma phase precipitation in deformed sample is found to be lower than that in undeformed sample.

Keywords phase diagram, preaging deformation, sigma phase precipitation, super duplex stainless steel

1. Introduction

Super duplex stainless steel (SDSS) belongs to a family of duplex stainless steels having a two-phase ferritic-austenitic microstructure (Ref 1). These steels, due to their high pitting resistance equivalent number (greater than 40), are considered to be distinct from other duplex stainless steel (DSS) (Ref 2–4). Because of their attractive combination of mechanical properties as well as corrosion resistance, they are widely used in nuclear reactors, and oil and gas industries (Ref 5, 6). Improved corrosion resistance and mechanical properties arise from a balance between the volume fraction of austenite and ferrite phase (Ref 7). However, during the various stages of manufacturing of products using SDSS, there exists a possibility of solid-state precipitation of several phases such as sigma, chi, pi, R, carbides, and nitrides, which lower the ductility, and reduce toughness and corrosion resistance (Ref 2, 7–11).

Sigma phase is known to have a tetragonal crystal structure ($c/a = 0.52$; 30 atoms per unit cell with $a = 0.880$ nm and $c = 0.454$ nm) and a space group symmetry of $P4_2/mnm$ (Ref 1, 12). Sigma, being a brittle intermetallic phase, has a deleterious effect on mechanical properties (Ref 13). Since sigma phase is rich in chromium and molybdenum, the growth of the sigma phase results in depletion of chromium and molybdenum in the vicinity of the growing precipitate. Hence, the precipitation of sigma phase results in reduced corrosion resistance (Ref 14, 15).

Researchers have shown an enhanced precipitation of sigma phase during hot working and they have ascribed this to the lattice defects introduced during hot working (Ref 16, 17). Cold working prior to aging has also been shown to have a

stimulating influence on sigma phase precipitation in duplex stainless steel (Ref 17, 18). A detailed study of precipitation kinetics of sigma phase in undeformed 2205 DSS was carried out by Badji et al. (Ref 19). Despite the several work in the literature, a comparative study on sigma phase precipitation in undeformed and deformed samples needs to be documented. The aim of the present research is to study the effect of deformation (cold rolling) on aging characteristics and to describe the precipitation kinetics of the sigma phase in 2507 SDSS. Cold working in the present work is done to introduce dislocations in the material and is intended to simulate the effect of residual stress arising during the fabrication processes (Ref 20).

2. Material and Experimental Procedure

A 13-mm-thick plate-shaped sample of 2507 SDSS was obtained for the present study. The chemical composition of this sample is given in Table 1. A pseudo binary phase diagram with variable Cr concentration was calculated using the Thermocalc software. Samples were solution annealed at 1050 °C for 1 h and quenched in water. They were subsequently aged at the temperature 700, 750, 800, and 850 °C for different times and quenched in water. Metallographic sample preparation involved mechanical grinding and polishing followed by electrolytic etching. The etchant was prepared by dissolving 10 g of KOH in 100 ml of distilled water. Microstructures were examined using Olympus optical microscope and Hitachi S-3400 Scanning Electron Microscope (SEM). X-ray diffraction studies were carried out using a PANalytical diffractometer. In all these studies, the incident radiation was Cu $K\alpha$ (1.54 Å), and the phase identification was performed using X'Pert HighScore Plus software. The volume fraction of the sigma phase was determined using Olympus image analysis software. In order to study the effect of sigma phase on mechanical properties, tensile samples were machined parallel to rolling direction of the plate. Tensile tests were carried out using Zwick Roell Amsler universal testing machine at room temperature and at an initial strain rate of 10^{-3} s $^{-1}$. The fracture surfaces were observed in SEM. Phase composition was determined using thermo Noran energy-dispersive x-ray (EDX) spectrometer attached to the SEM. In order to study

M.K. Mishra, A.G. Rao, B.P. Kashyap, and N. Prabhu, Department of Metallurgical Engineering and Materials Science, Indian Institute of Technology, Bombay, Mumbai 400076, India; and R. Sarkar, Research and Development, Tata Steel Limited, Jamshedpur 831001, India. Contact e-mail: manjeshkumar.mishra@gmail.com.

the effect of preaging deformation on kinetics of sigma phase precipitation, solution-annealed samples were cold rolled to 60% deformation in various passes and then aged over the temperature range of 700-850 °C for different times. All heat treatments were carried out in a muffle furnace having a temperature control of ± 2 °C.

3. Results and Discussion

3.1 Microstructure Evolution During Aging of Undeformed Samples

Figure 1 shows the pseudo binary phase diagram of super duplex stainless steel in the temperature range of 800-1300 °C calculated using thermocalc software and TC-Fe7 data base. The dotted line superimposed on the phase diagram indicates the bulk composition of steel. It can be seen that at high temperatures in the range 975 to 1040 °C, three phases viz., austenite, ferrite, and sigma are in equilibrium with each other. Between 975 and 950 °C, two phases austenite and sigma coexist, and at temperatures below 950 °C, three phases austenite, epsilon (Cr_2N), and sigma are in equilibrium.

Figure 2 shows the optical micrographs of samples, solution annealed and aged at 850 °C for different times. From these micrographs, it is clear that as aging time increases, the fraction of sigma phase (brown in color) increases. The sigma phase has been reported to form through a cooperative eutectoid reaction of the type $\alpha \rightarrow \sigma + \gamma_2$, where α , σ , and γ_2 are ferrite, sigma, and secondary austenite, respectively (Ref 9). Elmer et al. (Ref 21) suggested that the secondary austenite nucleates first at ferrite/austenite boundaries causing excess chromium and molybdenum to be rejected into the ferrite ahead of the secondary austenite. As the concentration of these elements in the ferrite phase increases, the driving force for precipitation of sigma phase increases. The sigma phase subsequently nucleates and grows either along the secondary austenite or as isolated islands surrounded by secondary austenite.

The pseudo binary phase diagram (Fig. 1) shows that at temperatures below 950 °C, epsilon phase (Cr_2N) also co-exists along with austenite and sigma phase. Careful TEM studies in the literature revealed the precipitation of intergranular and intragranular Cr_2N precipitates (Ref 2). The volume fraction of Cr_2N precipitates was estimated to be 0.4% even after long-term aging of 1008 h at 850 °C (Ref 22).

Figure 3 shows the x-ray diffractograms obtained from samples, solution annealed and aged at 850 °C for different times. It can be seen that as aging progresses, the intensity peak from ferrite phase decreases and the intensity peaks from the sigma phase and the austenite phase increase. This further confirms that as aging progresses, ferrite phase transforms to a mixture of sigma and secondary austenite phases. It may be noted that the intensity peaks from sigma phase could be just identified in samples aged for a duration of 15 min at 850 °C.

Figure 4 shows the x-ray diffractograms obtained from samples, solution annealed and aged at 750 °C for different

times. The intensity peaks from sigma phase could be just identified only after prolonged aging for 1 h. This is in contrast to the result obtained in samples aged at 850 °C.

3.2 Tensile Properties of Undeformed and Aged Samples

Figure 5 shows engineering stress-engineering strain curves obtained after tensile testing of samples, solution annealed, and aged at 850 °C for different times. It can be seen that as the aging time increases, ductility decreases with simultaneous increase in yield strength. Solution-annealed sample displayed a yield strength of 600 MPa and elongation of 45%, whereas sample aged for 3 h at 850 °C displayed a yield strength more than 1100 MPa and negligible ductility. These changes in tensile properties can be attributed to the transformation of softer ferrite phase into the harder sigma phase.

Figure 6 shows the fractographs of samples in different conditions. It is clear from the fractographs that in the samples aged at 850 °C for longer duration, the area occupied by the flat facets increases and the area occupied by the dimples decreases, indicating progressive brittleness induced by formation of the sigma phase. This is further confirmed by observation of cracks in the sigma phase as shown in Fig. 7. EDS studies indicate sigma phase to be richer in chromium and molybdenum, while austenite is richer in nickel and manganese (Table 2).

3.3 Microstructural Evolution During Aging of Deformed Samples

Figure 8 shows the microstructures obtained from samples, solution annealed, cold rolled to 60% deformation, and then aged at 850 °C for different times. Similar to the microstructures obtained from undeformed samples described in section 3.1, the microstructures obtained from the deformed samples also show the transformation of ferrite phase into a mixture of sigma phase and secondary austenite. However, it

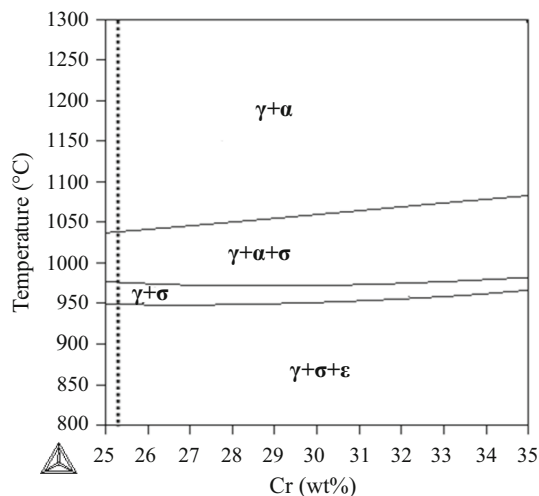


Fig. 1 Pseudo binary phase diagram

Table 1 Chemical composition of the 2507 SDSS sample

Elements	C	S	P	Mn	Si	Cr	Ni	Mo	Cu	N	Fe
wt.%	0.016	0.003	0.023	0.72	0.25	25.20	6.9	3.79	0.19	0.26	Balance

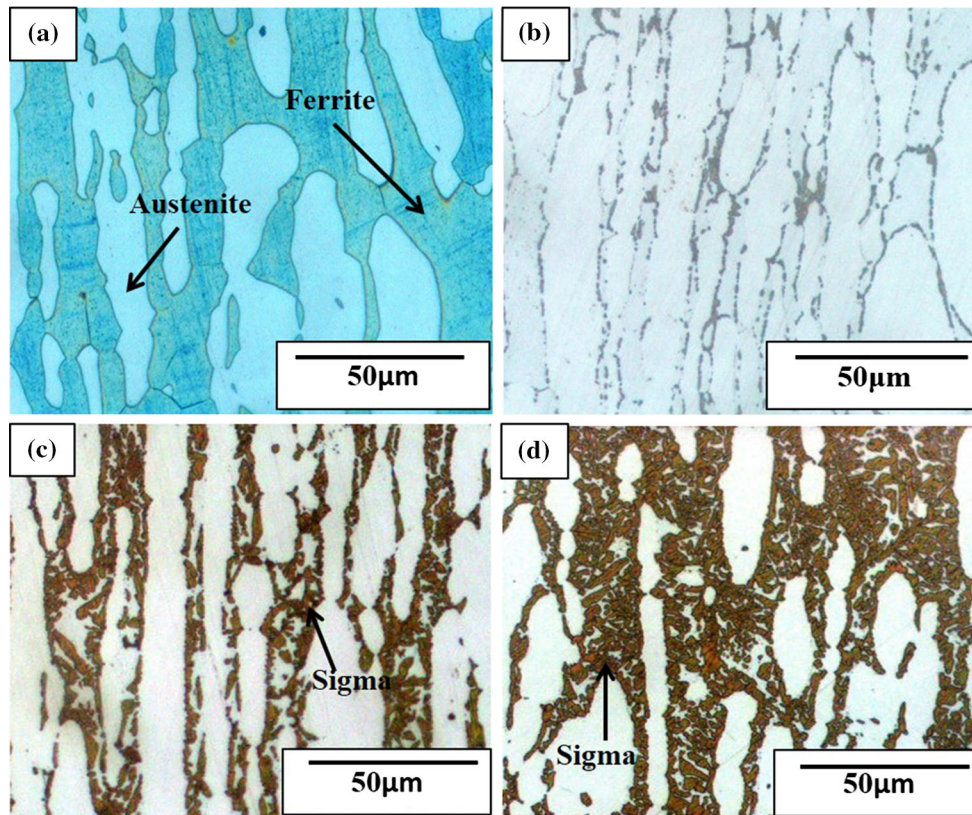


Fig. 2 Optical micrographs of different samples (a) solution annealed; solution annealed and aged at 850 °C for different times (b) 5 min (c) 1 h and (d) 3 h

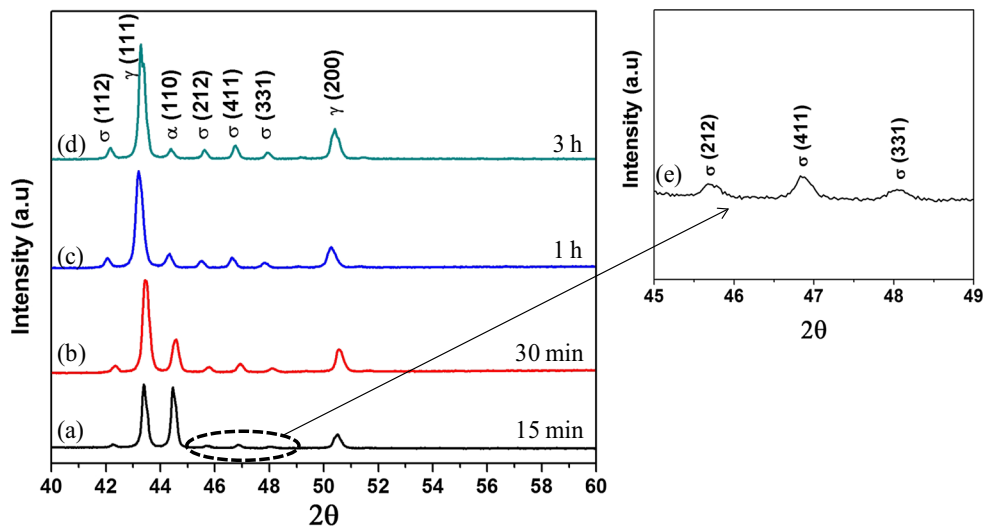


Fig. 3 X-ray diffractograms obtained from samples, solution annealed and aged at 850 °C for different times (a) 15 min (b) 30 min (c) 1 h (d) 3 h and (e) enlarged view of the diffractogram shown in (a)

may be noted that in case of deformed samples, the transformation is very rapid and goes to completion in about 30 min.

Figure 9 compares the x-ray diffractograms obtained from undeformed and deformed samples aged at 750 °C for 30 min and 1 h. It can be seen that in deformed samples, the intensity

of the ferrite peak has reduced, while intensity of sigma and austenite peaks has increased substantially. These results clearly indicate that preaging deformation leads to accelerated transformation kinetics. As austenite-ferrite interfaces (average grain thickness in undeformed and deformed samples are

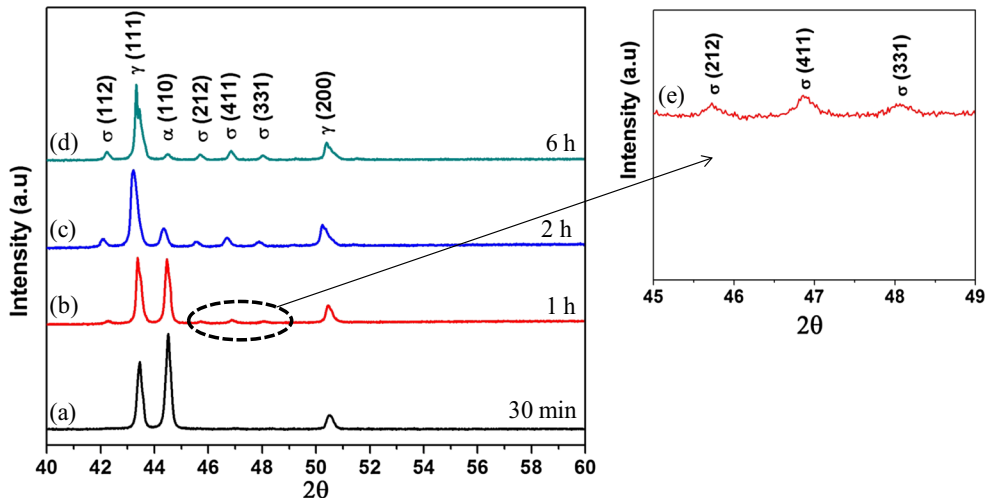


Fig. 4 X-ray diffractograms obtained from samples, solution annealed and aged at 750 °C for different times (a) 30 min (b) 1 h (c) 2 h (d) 6 h and (e) enlarged view of the diffractogram shown in (b)

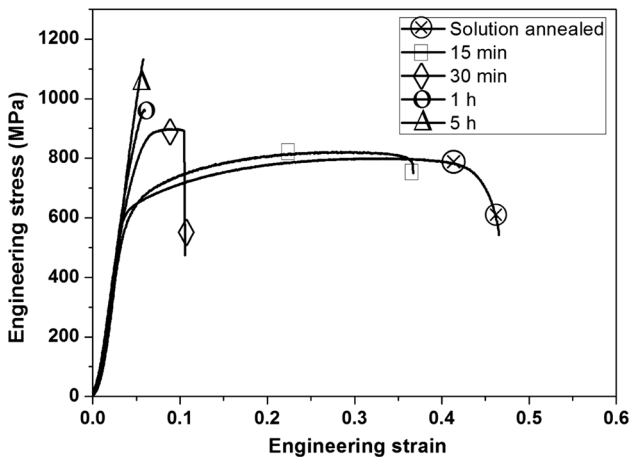


Fig. 5 Engineering stress-engineering strain curves obtained from samples solution annealed and aged at 850 °C for different times

approximately 16 and 6 μm , respectively) are potential sites for nucleation of sigma phase, any increase in the interfacial area per unit volume would result in increased nucleation kinetics (Ref 6, 11, 23). Further, the growth rates are also enhanced due to increased diffusivity along the interfaces and the dislocations generated during deformation (Ref 17).

3.4 Precipitation Kinetics

Figure 10 shows the volume fraction of sigma phase as a function of time at different aging temperature. The fraction of sigma phase increases with increasing time in both undeformed and deformed samples. In deformed sample at aging temperature of 850 °C, the transformation $\alpha \rightarrow \sigma + \gamma_2$ is almost completed after 30 min, whereas in undeformed sample, the transformation is completed in 3 h.

Johnson-Mehl-Avrami-Kolmogorov (JMAK) equation is used extensively to study the kinetics of the phase transformation. This theory has been used frequently in the literature where nucleation and growth take place such as during diffusion controlled precipitation, recrystallization, and ferroelectric/ferromagnetic switching. (Ref 24). The classical model of the JMAK equation (Ref 25) is given below.

$$y(t) = 1 - \exp(-(kt)^n), \quad (\text{Eq 1})$$

where $y(t)$, k , and n are the volume fraction of phase transformed in time t , reaction rate constant, and Avrami exponent, respectively. This classical JMAK model has been used to study the kinetics of sigma phase transformation in duplex stainless steel (Ref 1, 26, 27). However, Badji et al. (Ref 19) reported that the classical JMAK model does not describe accurately the precipitation kinetics of sigma phase since it is unable to account for the experimental data observed toward the end of the transformation. Starink (Ref 24) suggested that Gibbs-Thomson (or capillary) effect, vacancy annihilation, blocking due to anisotropic growth, internal stresses, and impingement on defects are the possible causes for deviation. A modified JMAK transformation kinetics equation was adopted by Badji et al. (Ref 19) to study the kinetics of sigma phase precipitation in undeformed and aged 2205 DSS samples. The modified equation has following form:

$$\frac{dy}{dt} = nk^n t^{(n-1)} (1-y)^{(1+c)}, \quad (\text{Eq 2})$$

where c is the impingement parameter. The integration of the above equation gives

$$y = 1 - \left[\frac{1}{1 + c(kt)^n} \right]^{\frac{1}{c}}, \quad (\text{Eq 3})$$

where c is not equal to zero (Eq 3), and upon rearranging, the following equation is obtained.

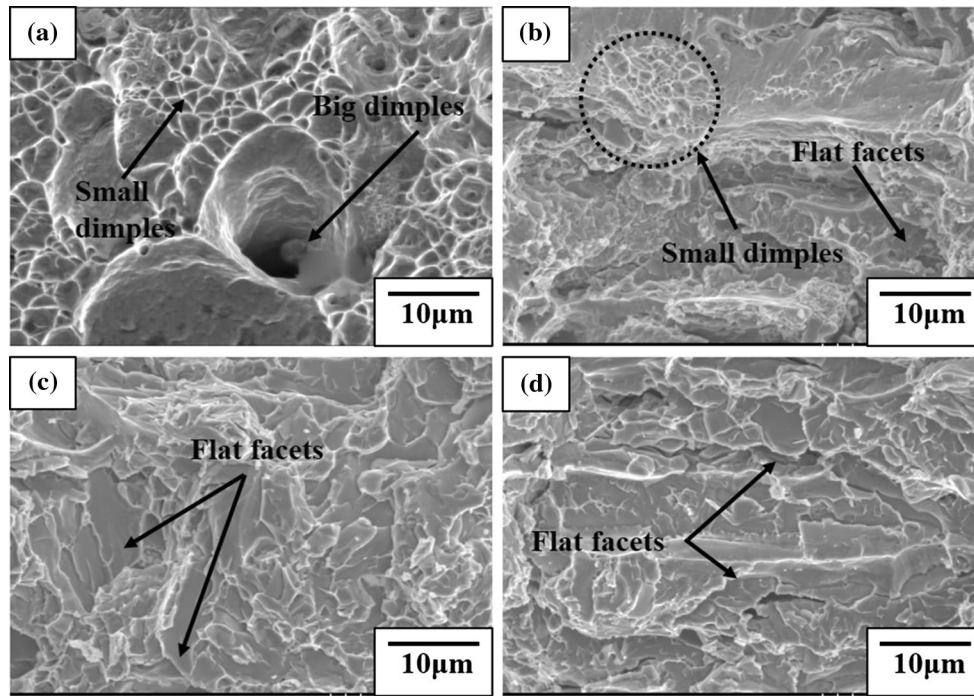


Fig. 6 Fractographs of samples in different conditions (a) solution annealed; solution annealed and aged at 850 °C for different times (b) 30 min (c) 1 h and (d) 3 h

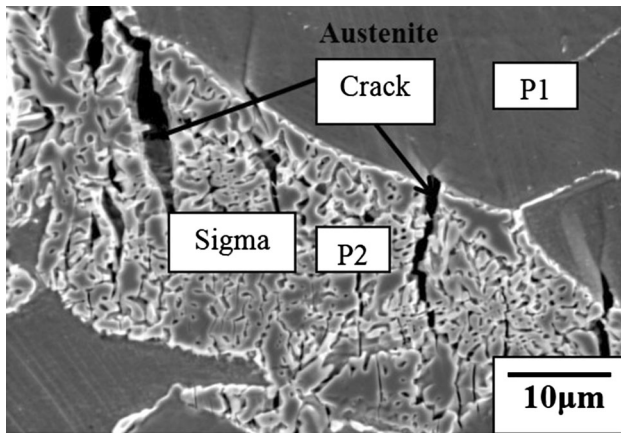


Fig. 7 Secondary electron micrograph taken near the fracture surface of tensile sample aged at 850 °C for 3 h

Table 2 Chemical compositions (approximate) of austenite phase and sigma phase obtained by EDS at locations P1 (austenite) and P2 (sigma phase) shown in Fig. 7

Elements, wt.%	Cr	Mo	Ni	Mn	Si	Fe
P1 (austenite)	24.33	2.47	7.99	0.85	0.38	Balance
P2 (sigma phase)	28.25	12.31	2.65	0.69	0.54	Balance

$$n \ln(k) + n \ln(t) = \ln \left[\frac{(1-y)^{-c} - 1}{c} \right]. \quad (\text{Eq 4})$$

To obtain a good correlation between experimental results and the model, the value of impingement parameter c is varied.

The best correlation (R^2 greater than 0.95) was obtained upon using a value of $c = 0.5$. Figure 11 shows the plot of $\ln \left[\frac{(1-y)^{-c} - 1}{c} \right]$ versus $\ln(t)$. The Avrami exponent n is found from the slope of the line, and the intercept provides information about rate constant k .

The average values of Avrami exponent found in undeformed and deformed samples were 1.60 and 1.65, respectively. Badji et al. (Ref 19) have also reported a value of n close to 1.5 for the sigma phase precipitation in undeformed and aged 2205 DSS. Table 3 lists the values of the reaction rate constants obtained for undeformed and deformed samples.

The activation energy in the temperature range of 700–850 °C was calculated using the Arrhenius equation,

$$k = k_0 \exp \left(-\frac{Q}{RT} \right), \quad (\text{Eq 5})$$

where k_0 is the pre-exponential constant, Q is the activation energy for the transformation, R is the universal gas constant, and T is the absolute temperature. A plot of $\ln(k)$ versus $1/T$ shown in Fig. 12 gives the value of activation energy. The activation energies for sigma phase formation in undeformed and deformed samples were found to be 116.89 and 95.69 kJ/mol, respectively. In undeformed and aged UNS S31803 DSS, Magnabosco (Ref 22) reported an activation energy value of 185 kJ/mol. This value is higher than the present value possibly due to increased amount of chromium and molybdenum in 2507 SDSS compared to UNS S31803 DSS. This is consistent with the fact that the precipitation rate of the sigma phase increases with increase in the content of sigma forming elements chromium and molybdenum, in steel, especially in α -phase where most of the sigma phase precipitates (Ref 17).

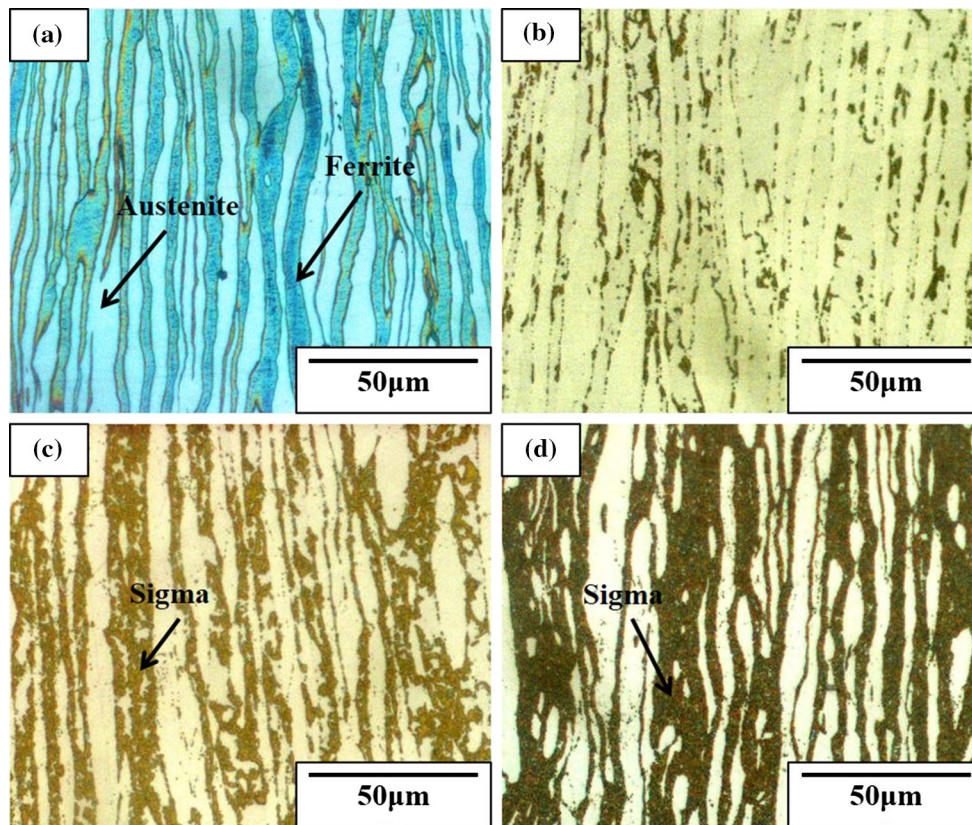


Fig. 8 Optical micrographs of the different samples (a) solution annealed and deformed (60% cold rolled); solution annealed, deformed (60% cold rolled) and aged at 850 °C for different times (b) 2 min (c) 10 min and (d) 30 min

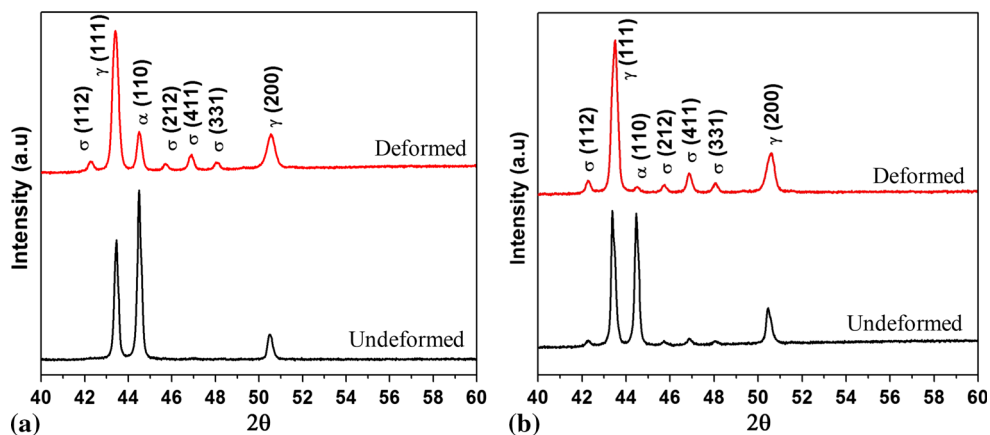


Fig. 9 X-ray diffractograms obtained from samples aged at 750 °C for different times (a) 30 min and (b) 1 h

The activation energy for diffusion of molybdenum in ferrite is 289 ± 13 kJ/mol and for chromium in ferrite is 235 ± 15 kJ/mol (Ref 22). The activation energy for sigma phase precipitation obtained in the present work (for both undeformed and deformed sample) is lower than the activation energy for the diffusion of chromium and molybdenum in ferrite. Thus, the transformation $\alpha \rightarrow \sigma + \gamma_2$ in SDSS is not

controlled by the chromium as well as molybdenum diffusion in the ferrite. This leads to the inference that interface reaction is the main mechanism which controls the sigma phase precipitation in undeformed and deformed sample. Badji et al. (Ref 19) have also reported that the ferrite to sigma phase precipitation in undeformed and aged 2205 DSS is controlled by the interface reaction.

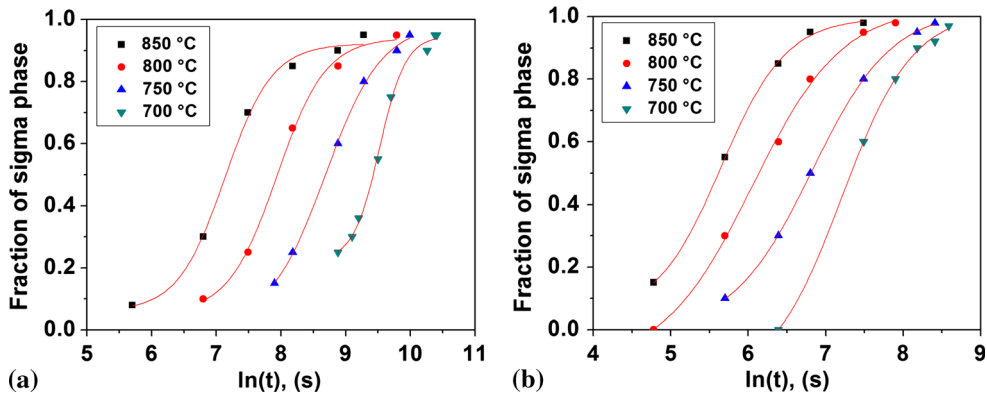


Fig. 10 Fraction of sigma phase as a function of aging time in (a) undeformed samples and (b) deformed samples

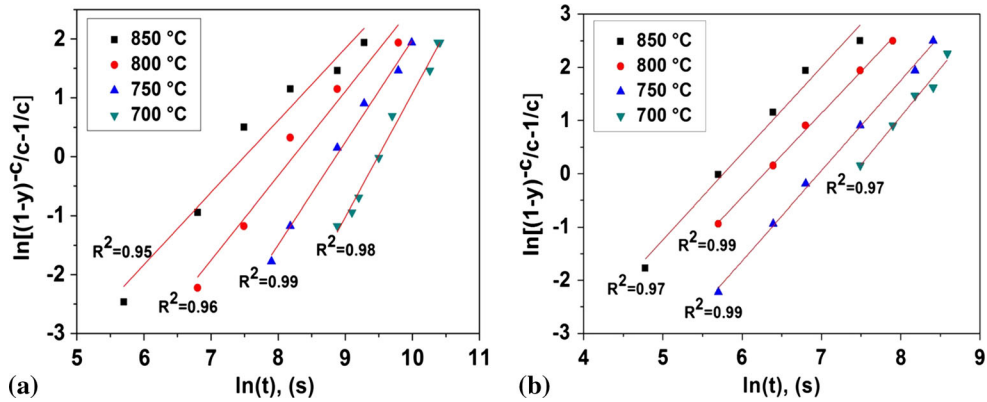


Fig. 11 $\ln\left[\frac{(1-y)^{-c}-1}{c}\right]$ as a function of $\ln(t)$ for (a) undeformed samples and (b) deformed samples

Table 3 Reaction rate constants for sigma phase precipitation

Temperature, °C	Reaction rate constant, k , s^{-1}	
	Undeformed	Deformed
850	5.1×10^{-4}	2.9×10^{-3}
800	2.3×10^{-4}	1.5×10^{-3}
750	1.2×10^{-4}	9.6×10^{-4}
700	7.3×10^{-5}	5.8×10^{-4}

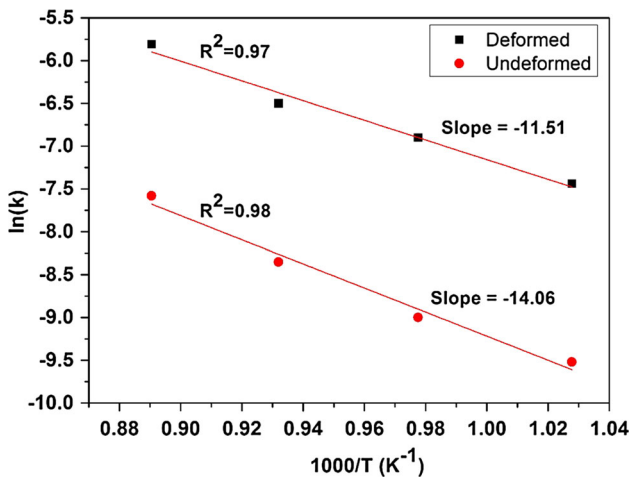


Fig. 12 Plot of $\ln(k)$ vs. $1/T$

4. Conclusions

Following are the main conclusions drawn from this work on aging behavior of 2507 super duplex stainless steel.

1. The fraction of sigma phase formed in undeformed sample as a result of the transformation $\alpha \rightarrow \sigma + \gamma_2$ increases with increasing time, and at 850 °C, the transformation goes to completion after 3 h.
2. As the fraction of sigma phase increases in the microstructure, ductility decreases with simultaneous increase in yield strength. Solution-annealed sample displayed a yield strength of 600 MPa and elongation of 45%, whereas sample aged for 3 h at 850 °C displayed a yield strength more than 1100 MPa and negligible ductility. During tensile deformation, cracks are observed to initiate in the sigma phase.

3. Preaging deformation results in accelerated sigma phase precipitation, and at 850 °C, the transformation $\alpha \rightarrow \sigma + \gamma_2$ is completed after 30 min.
4. The precipitation kinetics of sigma phase is found to obey the modified JMAK model. The activation energy for sigma phase precipitation in deformed sample is lower than that in undeformed sample.

Acknowledgments

We would like to thank the Department of Science and Technology, India, for funding under FIST program SR/FST/ETII-054/2000 for purchase of Universal Testing Machine.

References

1. S. Byun, N. Kang, T. Lee, S. Ahn, H.W. Lee, W. Chang, and K. Cho, Kinetics of Cr/Mo-Rich Precipitates Formation for 25Cr-6.9Ni-3.8Mo-0.3N Super Duplex Stainless Steel, *Met. Mater. Int.*, 2012, **18**, p 201–207
2. J. Nilsson, Overview Super Duplex Stainless Steels, *Mater. Sci. Technol.*, 1992, **8**, p 685–700
3. A.R. Akisanya, U. Obi, and N.C. Renton, Effect of Ageing on Phase Evolution and Mechanical Properties of a High Tungsten Super-Duplex Stainless Steel, *Mater. Sci. Eng. A*, 2012, **535**, p 281–289
4. H.J. Park and H.W. Lee, Study on Cracking Characteristics on Aging of Super Duplex Stainless Steel Weld Metal, *Mater. Sci. Technol.*, 2014, **30**, p 377–384
5. K. Ravindranath and S.N. Malhotra, The Influence of Aging on the Intergranular Corrosion of 22 Chromium 5 Nickel Duplex Stainless Steel, *Corros. Sci.*, 1995, **37**, p 121–132
6. S. Jeon, S. Kim, S. Kim, M. Choi, and Y. Park, Effects of Solution-Annealing Temperature on the Precipitation of Secondary Phases and the Associated Pitting Corrosion Resistance in Hyper Duplex Stainless Steel, *Mater. Trans.*, 2013, **54**, p 1473–1479
7. C. Huang and C. Shih, Effects of Nitrogen and High Temperature Aging on σ Phase Precipitation of Duplex Stainless Steel, *Mater. Sci. Eng. A*, 2005, **402**, p 66–75
8. M. Martins and L.R.N. Forti, Effect of Aging on Impact Properties of ASTM A890 Grade 1C Super Duplex Stainless Steel, *Mater. Charact.*, 2008, **59**, p 162–166
9. D.M.E. Villanueva, F.C.P. Junior, R.L. Plaut, and A.F. Padilha, Comparative Study on Sigma Phase Precipitation of Three Types of Stainless Steels: Austenitic, Superferritic and Duplex, *Mater. Sci. Technol.*, 2006, **22**, p 1098–1104
10. A.F. Padilha, D.J.M. Aguiar, and R.L. Plaut, Duplex Stainless Steels: A Dozen of Significant Phase Transformations, *Defect Diffus. Forum*, 2012, **322**, p 163–174
11. T.H. Chen and J.R. Yang, Effects of Solution Treatment and Continuous Cooling on σ -Phase Precipitation in a 2205 Duplex Stainless Steel, *Mater. Sci. Eng. A*, 2001, **311**, p 28–41
12. T. Lee, S. Kim, and S. Takaki, Time-Temperature-Precipitation Characteristics of High Nitrogen Austenitic Fe-18Cr-18Mn-2Mo-0.9N Steel, *Metall. Mater. Trans. A*, 2006, **37**, p 3445–3454
13. M. Pohl, O. Storz, and T. Glogowski, Effect of Intermetallic Precipitations on the Properties of Duplex Stainless Steel, *Mater. Charact.*, 2007, **58**, p 65–71
14. B. Deng, Y.M. Jiang, J. Gao, and J. Li, Effect of Annealing Treatment on Microstructure Evolution and the Associated Corrosion Behavior of a Super-Duplex Stainless Steel, *J. Alloys Compd.*, 2010, **493**, p 461–464
15. B. Deng, Z. Wang, Y. Jiang, H. Wang, J. Gao, and J. Li, Evaluation of Localized Corrosion in Duplex Stainless Steel Aged at 850 °C with Critical Pitting Temperature Measurement, *Electrochim. Acta*, 2009, **54**, p 2790–2794
16. A. Momeni and K. Dehghani, Effect of Hot Working on Secondary Phase Formation in 2205 Duplex Stainless Steel, *J. Mater. Sci. Technol.*, 2010, **26**, p 851–857
17. Y. Maehara, N. Fujino, and T. Kunitake, Effects of Plastic Deformation and Thermal History on σ -Phase Precipitation in Duplex Phase Stainless Steels, *Trans. ISIJ*, 1983, **23**, p 247–255
18. H. Cho and K. Lee, Effect of Cold Working and Isothermal Aging on the Precipitation of Sigma Phase in 2205 Duplex Stainless Steel, *Mater. Charact.*, 2013, **75**, p 29–34
19. R. Badji, N. Kherrouba, B. Mehdi, B. Cheniti, M. Bouabdallah, C. Kahloun, and B. Bacroix, Precipitation Kinetics and Mechanical Behavior in a Solution Treated and Aged Dual Phase Stainless Steel, *Mater. Chem. Phys.*, 2014, **148**, p 664–672
20. S. Sathyanarayanan, J. Basu, A. Moitra, G. Sasikala, and V. Singh, Effect of Thermal Aging on Ductile-Brittle Transition Temperature of Modified 9Cr-1Mo Steel Evaluated with Reference Temperature Approach Under Dynamic Loading Condition, *Metall. Mater. Trans. A*, 2013, **44**, p 2141–2155
21. J.W. Elmer, T.A. Palmer, and E.D. Specht, Direct Observations of Sigma Phase Formation in Duplex Stainless Steels Using In-Situ Synchrotron X-ray Diffraction, *Metall. Mater. Trans. A*, 2007, **38**, p 464–475
22. R. Magnabosco, Kinetics of Sigma Phase Formation in a Duplex Stainless Steel, *Mater. Res.*, 2009, **12**, p 321–327
23. H. Sieurin and R. Sandström, Sigma Phase Precipitation in Duplex Stainless Steel 2205, *Mater. Sci. Eng. A*, 2007, **444**, p 271–276
24. M.J. Starink, On the Meaning of the Impingement Parameter in Kinetic Equations for Nucleation and Growth Reactions, *J. Mater. Sci.*, 2001, **36**, p 4433–4441
25. R. Badji, M. Bouabdallah, B. Bacroix, C. Kahloun, K. Bettahar, and N. Kherrouba, Effect of Solution Treatment Temperature on the Precipitation Kinetic of σ -Phase in 2205 Duplex Stainless Steel Welds, *Mater. Sci. Eng. A*, 2008, **496**, p 447–454
26. I. Calliari, M. Zanesco, and E. Ramous, Influence of Isothermal Aging on Secondary Phases Precipitation and Toughness of a Duplex Stainless Steel SAF 2205, *J. Mater. Sci.*, 2006, **41**, p 7643–7649
27. N.O. Lara, A. Ruiz, C. Rubio, R.R. Ambriz, and A. Medina, Nondestructive Assessing of the Aging Effects in 2205 Duplex Stainless Steel Using Thermoelectric Power, *NDT E Int.*, 2011, **44**, p 463–468